Solution Behavior of Trimethylsilyl Cellulose of Different Degrees of Substitution, Studied by Static and Dynamic Light Scattering

Jürgen Demeter,[†] Werner Mormann,[†] Jürgen Schmidt,[‡] and Walther Burchard*[,‡]

Fachbereich 8, Laboratory of Macromolecular Chemistry, University of Siegen, 57068 Siegen, Germany, and Institute of Macromolecular Chemistry, University of Freiburg, 79104 Freiburg, Germany

Received January 14, 2003; Revised Manuscript Received May 13, 2003

ABSTRACT: Eight samples of trimethylsilyl cellulose (TMSC) with different degrees of substitution (DS) were investigated by static and dynamic light scattering in tetrahydrofuran at 25 °C. Six of these sample were prepared from Avicel cellulose ($DP_w = 221$) by controlled silylation with stoichiometric amounts of hexamethyldisilazane in liquid ammonia at elevated temperature in an autoclave. The two others were obtained by controlled desilylation of the sample with DS = 2.72. The TMSC samples were soluble in tetrahydrofuran, but in all cases strong aggregation was observed with aggregation numbers of 80 for DS = 1.96 up to 270 for DS = 2.72. Surprisingly, the aggregation number considerably increased for the samples obtained by desilylation. These very large aggregates permitted a detailed analysis of the angular dependencies which resulted in rather rigid structures with Kuhn segment lengths of $l_K = 122-174$ nm, about 6 times the segment length of molecularly dissolved cellulose derivatives. This increase in chain stiffness is caused by a side-by-side alignment of 2−4 chains, which further increased to about 13−14 chains for the samples obtained by partial desilylation. The structure of the aggregates resembles that of branched macromolecules built up from stiff chains in which the junction zones of 2−4 aligned chains act as branching points.

Introduction

The synthesis of trimethylsilyl cellulose (TMSC) derivatives started already in 1948 with the work by Schuyten et al.[1] Silylation of cellulose has been used and studied by a number of researchers[2,3] (further references therein) and was recently reviewed by Mormann[4] and Petzold et al.[5] Silylation in liquid ammonia with hexamethyldisilazane (HMDS) at 80 °C in an autoclave[6] enabled us to obtain TMSC with full substitution to DS = 3.0.[2] Also, the synthesis of TMSC to predictable degrees of substitution became possible.[3] Finally, a controlled desilylation of TMSC could be achieved with stoichiometric amounts of water in a mixture of ammonia and tetrahydrofuran (THF).[7]

Partially substituted TMSC is soluble in THF if the degree of substitution is above 1.5. Solubility seemed to improve with increasing DS but decreased again at high DS. Fully substituted cellulose (DS = 3.0) gave only 3% of THF extractable material. The solubility depended on the degree of polymerization. Similar peculiar solubility behavior is also known for other cellulose derivatives, e.g., cellulose acetates studied by Kamide and Saito 1984[8] and by Schulz et al.[9] This behavior is not well understood. To bring some light into this phenomenon, we started a systematic physical−chemical study on the DS dependence of some cellulose trimethylsilyl derivatives.

Using the synthetic routes mentioned above, trimethylsilyl celluloses of different degrees of silylation were prepared from microcrystalline celluloses, Avicel 101 and Avicel 102. Size exclusion chromatography (SEC) of some TMSC gave evidence for aggregation.[2] To find the chain length of the Avicel samples, the tricarbanilate derivatives were prepared and measured in THF by SEC in combination with multiangle laser light scattering (MALLS). For both Avicel samples a DP = 220 ± 6 was found. In this study we also included samples obtained by partial desilylation of a highly substituted TMSC (DS 2.72). It was of interest to learn whether this reverse method of preparation had an influence on the extent of aggregation.

In this paper we present results obtained from a combination of static and dynamic light scattering from TMSC of different degrees of silylation.

Experimental Section

Materials. The synthesis and most of the trimethylsilyl cellulose samples used in the present study have been described in previous papers,[2−4] and the details will not be repeated here.

Static Light Scattering. Static LS measurements were made with a computer-driven modified SOFICA photogoniometer. A 5 mW HeNe laser (Uniphase) was used as light source. For each concentration the scattering intensity was recorded at 24 different angles in a range from 30° to 145° in steps of 5°. Mostly five different concentrations were measured which were prepared from a stock solution by dilution. The various solutions were filtered through 5 μm filters (Satorius, Göttingen) and finally transferred into cylindrical scattering cells of 8 mm i.d. and 70 mm length. Only in one case (sample 5) was a 0.5 μm filter used, which however led to a strong reduction in the molar mass (see Table 1). The cells, made of special glass, were sealed with a Teflon stopper. Before use, the light scattering cells were carefully made dust free by rinsing with freshly distilled acetone in a special fountain-like apparatus (Dinkelacker, Mainz, Germany).

The scattering data are commonly plotted in the form of a Zimm plot,[10] i.e., Kc/R_θ against $q^2 + kc$. This plot is based on the well-known Debye relationship

$$\frac{Kc}{R_\theta} = \frac{1}{M_w P(\theta)} + 2A_2c + \ldots \cong \frac{1 + (1/3)R_g^2q^2 - \text{higher terms in } q^2}{M_w} + 2A_2c \quad (1)$$

[†] University of Siegen.
[‡] University of Freiburg.
* Corresponding author: e-mail walther.burchard@makro.uni-freiburg.de.

10.1021/ma0300286 CCC: $25.00
Published on Web 06/18/2003

Table 1. Molecular Parameters of Trimethylsilyl Celluloses from Silylation (Silyl) and Desilylation (Desilyl) Measured by Static and Dynamic Light Scattering in THF at 25 °C[a]

no.	DS	tye	$M_w \times 10^{-6}$, g/mol	$A_2 \times 10^6$, mol mL/g^2	R_g, nm	R_h, nm	$\rho = R_g/R_h$	aggr no.	$d_{app} \times 10^3$, g/mL
1	1.78	desilyl	18.1	+3.75	157			302	1.854
2	1.86	desilyl	52.7	−0.527	176	768	0.23	808	3.832
3	1.96	silyl	5.48	−3.60	184	643	0.29	82	0.335
4	2.12	silyl	6.14	−10.8	188			89	0.366
5[b]	2.37	silyl	0.143	+324.0	37	31	1.19	2[b]	1.119
6	2.37	silyl	9.27	+0.71	202	634	0.32	126	0.446
7	2.72	silyl	21.3	−0.551	205	549	0.37	270	0.980
8[c]	3.00	silyl	164.		359			20650[c]	9.97

[a] DS = degree of substitution; M_w = weight-average of the molar particle weight, R_g and R_h = the radius of gyration and hydrodynamic radius, respectively; $\rho = R_g/R_h$ characteristic structure parameter; aggregation number: aggr no. = DP_w(LS)/DP_w(cellulose) and apparent density $d_{app} = 3M_w/(N_a\, 4\pi R_g^3)$. [b] Filtered through 0.5 μm pore size, all other samples were filtrated through 5 μm filters. [c] Extracted sol fraction from the mainly insoluble sample.

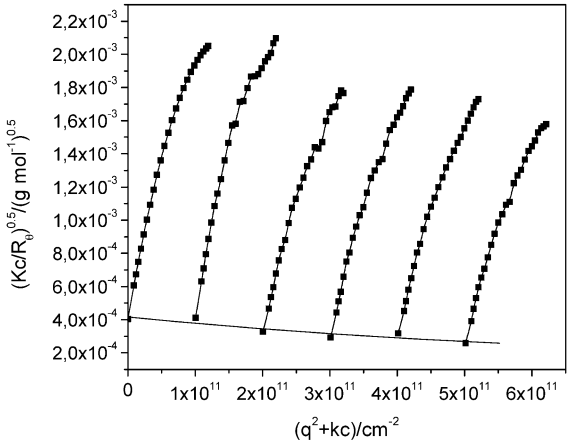

Figure 1. Berry plot of the static light scattering data from TMSC 7 measured in THF at 25 °C.

R_θ is the angular dependent Rayleigh ratio (normalized scattering intensity) and K the contrast factor of the macromolecule over the solvent which is proportional to $(dn/dc)^2$, the square of the refractive index increment. Its value was measured with a Brice-Phenix instrument in THF. M_w is the weight-average molar mass of the particles and

$$P(\theta) \equiv i(\theta)/i(\theta{=}0) \tag{2}$$

is the particle scattering factor. The parameter

$$q = (4\pi n_0/\lambda_0)\, \sin(\theta/2) \tag{3}$$

represents the magnitude of the scattering vector with θ the scattering angle, n_0 the solvent refractive index, and λ_0 the wavelength of the laser light in a vacuum. The radius of gyration is denoted as R_g, and A_2 is the second osmotic virial coefficient.

In the Zimm plot each curve from a certain concentration is shifted on the abscissa toward higher values by a factor that is proportional to the concentration. The parameter k is a freely eligible suitable constant to achieve good separation of the curves. The angular dependencies showed a marked upturn, which made the common extrapolation inaccurate in a Zimm plot. Therefore, a modification of the Zimm plot, as suggested by Berry,[11] was applied where the square root $(Kc/R_\theta)^{1/2}$ is plotted against $q^2 + kc$. This plot gave a good linear initial part and permitted a more accurate determination of the inverse molar mass.

Figure 1 shows a typical Berry plot of measurements from a trimethylsilyl cellulose with DS = 2.12. For each concentration the angular dependent data where extrapolated to scattering angle $\theta = 0$ (i.e., $q^2 = 0$), and each value at a selected scattering angle was extrapolated to zero concentration. The extrapolated curve at $c = 0$ no longer is influenced by interactions among the particles in solution. Three molecular parameters can be extracted from such a diagram: (1) the molar mass M_w, from the intercept which is $(1/M_w)^{1/2}$, (2) the root-mean-square radius of gyration R_g, from the initial slope of the curve at $c = 0$, which is $R_g^2/6M_w^{1/2}$, and (3) the second virial coefficient A_2, from the concentration dependence of the curve at scattering angle $\theta = 0$.

In view of the scatter of data at finite concentration the extrapolated angular dependence at $c = 0$ exhibits an unexpected high accuracy. This accuracy is a result of a smoothing algorithm in which the angular and concentration dependencies were approximated by polynomial fits. In the present cases a second-order polynomial gave already a satisfying fit. In addition, the algorithm took account of the fact that the curves at various concentrations only gradually change their shape with the concentration. Such smoothing proved to be useful for a further more detailed analysis as given below. The smoothed data were always checked by application of a Zimm plot, a Berry plot, and a modified Guinier plot. In the latter $\ln(Kc/R_\theta)$ is plotted against $q^2 + kc$. The fits were optimized such that in all cases approximately the same values for the molar mass and the radius of gyration were obtained. For the samples of those study the Berry plot gave a linearization of the initial part over a long q^2 region and permitted the highest accuracy in the determination of the radius of gyration. The estimated error (as printed out by the software) was about ±10% for the molar mass and 12% for the radius of gyration.

The curves of the angular dependence often have a characteristic shape which for large particles gives valuable information on the structure, i.e., whether it is a flexible or stiff chain, a randomly branched or a hyperbranched structure, or an aggregate. The normalized particle scattering factor $P(\theta)$ is used for interpretation (see Discussion).

Dynamic Light Scattering. In this technique a time correlation function of scattered light $g_2(q,c,t)$ is recorded in a time domain from 4×10^{-7} to 10^2 s. This time correlation function displays an exponential-like decay with a delay time whose initial part at short time can be described by the equation[12]

$$g_2(q,c,t) - 1 \cong B\, \exp(-2\Gamma t) \tag{4}$$

with

$$\Gamma = q^2 D_{app}(q,c) \tag{5}$$

In these equations the magnitude of the scattering vector q is defined in eq 3. The quantity $\Gamma/q^2 \equiv D_{app}(q,c)$ is an apparent translational diffusion coefficient that depends on scattering angle θ and concentration c. The true translational diffusion coefficient D is obtained after extrapolation of $D_{app}(q,c)$ to $q^2 = 0$ and $c = 0$. Applying the Stokes−Einstein relationship[13]

$$D = kT/(6\pi\eta R_h) \tag{6}$$

the hydrodynamic radius R_h is obtained.

Measurements were made with an ALV goniometer which was equipped with an ALV 5000 autocorrelator (ALV Laser

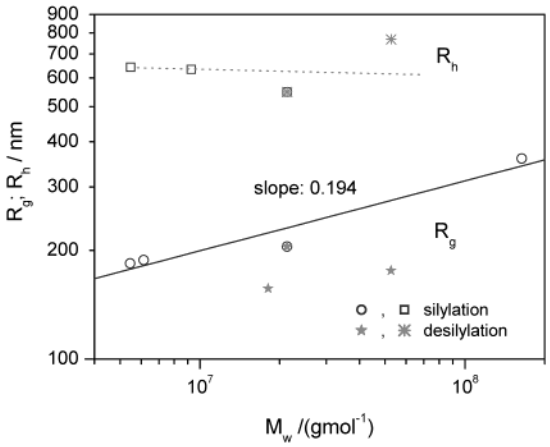

Figure 2. Radius of gyration R_g and hydrodynamic radius R_h as a function of the molar mass. Open symbols refer to silylated samples and asterisks to desilylated samples.

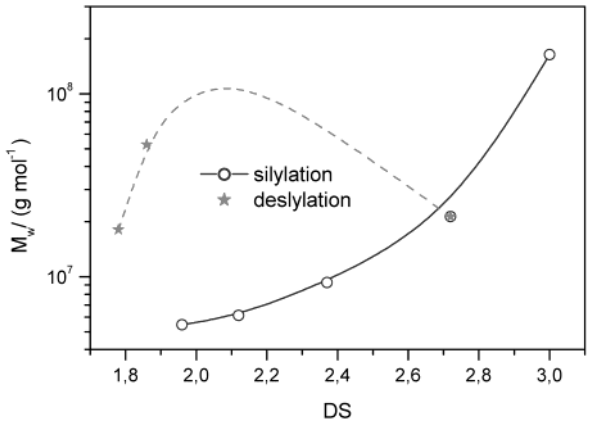

Figure 3. Increase of molar mass with degree of substitution. The samples were prepared from the same cellulose of DP_w = 221. Asterisks refer to desilylated samples. The dashed line is intended to guide the eye from the desilylated samples to that where they originated.

Vertrieb, Langen in Hessen, Germany). The red light of a Kr 2000 ion laser was used with λ_0 = 647 nm. The correlation functions were measured at 13 angles in steps of 10°. The same solutions and cylindrical cells were used as for static light scattering. The time correlation functions were evaluated for the diffusion coefficients via a so-called cumulant fit and also by a fit with stretched exponentials as suggested by Williams and Watts.[14] Furthermore, an inverse Laplace transformation was carried out with the CONTIN program by Provencher,[15] which resulted in a relaxation time distribution and finally a radii distribution. The viscosity of THF (η_0 = 0.47 mPa s at 20 °C) was taken to transform the diffusion coefficients into hydrodynamic radii (see eq 6). Examples of measured time correlation functions and the apparent radii distributions derived by the CONTIN inversion are shown in Figures 6 and 7.

Results

All measurements were carried out in THF at 20 °C. The results are listed in Table 1. A plot of R_g as a function of M_w is shown in Figure 2 in a double-logarithmic scale. The DS dependence is given in Figure 3. At this point it is important to emphasize that M_w is the molar *particle* mass and *not* the molecular mass of the macromolecule, and R_g is the corresponding radius of gyration. The second virial coefficient is a measure of interaction between the particles. A positive value indicates a good solvent in which the macromolecules repel each other. A negative value is observed for poor

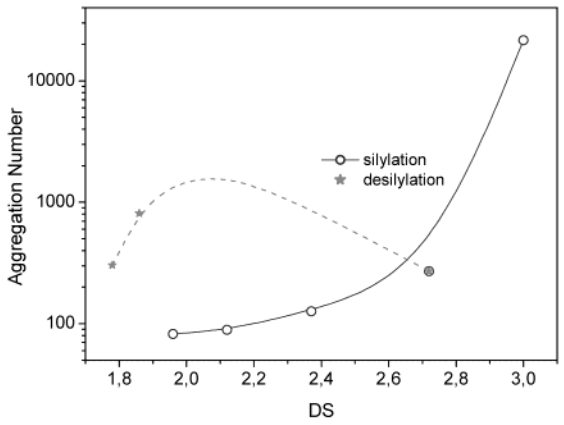

Figure 4. Correlation between the degree of substitution and the aggregation number.

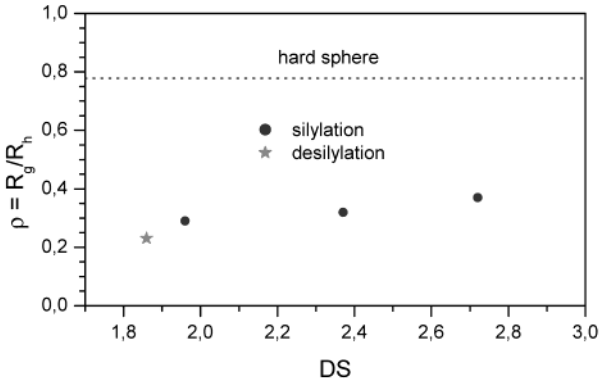

Figure 5. Dependence of the ρ parameter on the degree of substitution. The unusually low values indicate a micellar structure or a microgel with many dangling chains in the outer shell. This shell keeps the solvent partially captured, thus causing a much larger hydrodynamic radius than the radius of gyration.

solvents, but it also can indicate equilibrium association which proceeds with concentration. The values in Table 1 are mostly very small; the fluctuation between positive and negative values is probably insignificant and is within the experimental error.

Further insight into the structure of the particles can be obtained from the hydrodynamic radius that is obtained from dynamic light scattering measurements. These were performed only for a few examples. The data are again listed in Table 1 and plotted in Figures 2 and 3 as a function of molar mass and DS, respectively. The aggregation number as a function of DS was derived from the measured molar mass of the derivatives and the degree of polymerization of Avicel DP_w = 220. The result is presented in Figure 4. Furthermore, the ratio $\rho = R_g/R_h$ is plotted in Figure 5 as a function of DS. In this ratio the molar mass dependence largely cancels. It was of interest to compare the properties of a TMSC from silylation of cellulose to those of a sample obtained by desilylation of a TMSC high DS. This was done with sample 7 of DS = 2.72 and resulted in the samples TMSC 1 and 2 with DS 1.86 and DS 1.78, respectively. The data from these samples are included in the plots of Figures 2−4.

Discussion

Molar Mass Dependence. Although optically clear solutions were obtained, solution on a molecular level

was not achieved. It is common practice to plot the radius of gyration against the measured molar mass of the particles. Mostly a linear increase in the double-logarithmic plot is obtained which would indicate homologous behavior of the samples. Such behavior was indeed observed for the TMSC samples obtained through silylation but with an exceptionally low slope. The inverse slope follows the relationship

$$M_w \propto R_g^{d_f} \tag{7}$$

in which the exponent d_f represents a dimensionality of the particles. Values of $d_f = 3$, 2, and 1 can be expected for compact hard spheres, flat disks, and thin rigid rods, respectively. For less ordered structures the observed dimensions are no integers, and for this reason d_f is called a *fractal* dimension. In no case this dimension can be larger than 3.0. However, from the slope of 0.194 in Figure 2 an *apparent* fractal dimension of $d_{f,app} = 5.15$ would result which is physically meaningless and cannot be the fractal dimension of a single particle. Evidently, the particles grow very little in size whereas the particle weight increases extraordinarily. Such behavior indicates an increasing packing of the macromolecules caused by aggregation. Two possibilities are conceivable. The first is a side-by-side alignment of fairly rigid-rod-like macromolecules. In fact, the radius of gyration does not noticeably increase if thin rods are packed around each other in a regular way to form a cylinder. Such regular packing is unlikely; a staggered alignment is more reasonable which would involve a weak increase of the particle length and thus of the radius of gyration. The second model is based on even less ordered packing. On the other hand, it could not be the result of random aggregation. This type has been thoroughly studied in colloid science and is characterized by a fractal dimension of $d_f = 2.0-2.5$, depending on the quality of the solvent, i.e., whether the structure is highly swollen or in a state shortly before a collapse of the swollen structure.[16]

Surprisingly, the samples from desilylation show different behavior; their radii of gyration are smaller than those from the silylated TMSC with identical particle mass and degree of silylation. Apparently these samples are less swollen or more densely packed. The hydrodynamic radii are significantly larger than the radii of gyration and seem to have an opposite molar mass dependence, with a negative slope. Obviously, further information on the structure seems to be hidden in this behavior.

Dependence of Aggregation on DS. The increase of molar mass with DS in Figure 3 clearly shows that aggregation increases with the degree of substitution. Even for the lowest DS, where solubility was reached, aggregation numbers of around 80 were found which increased up to 270 for DS 2.72. The persilylated sample with DS 3.0 was actually not soluble. Only 3% could be extracted; probably this is the low molar mass fraction of Avicel with a DP lower than 200. The aggregation number of about 21 000 in Table 1 may still be an underestimation. These particles are tightly packed and scarcely swollen.

Again unexpected is the result of the desilylated samples. Instead of a decrease in the aggregation the opposite occurred. This could indicate nonrandom desilylation, where first the less ordered structures were attacked.

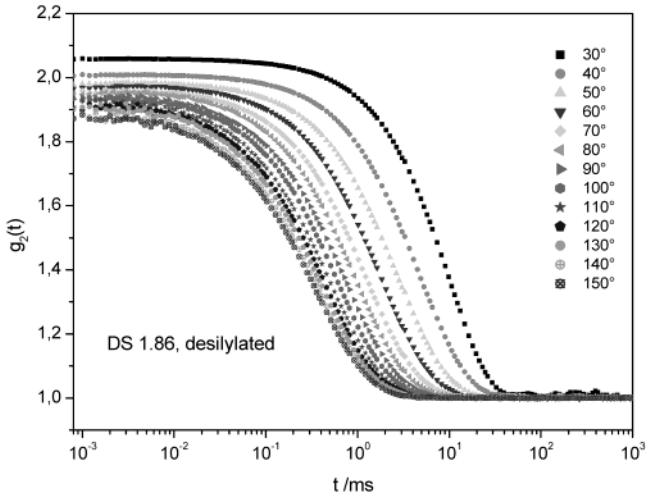

Figure 6. A set of intensity−time correlation function $g_2(t)$ obtained at 13 different scattering angles from dynamic light scattering of the desilylated sample TMSC 1. Note the smooth decay which gave no indication of a second slow mode.

Globular Structure of the Aggregates. *ρ Parameter*:[17,18] In contrast to the radius of gyration, the hydrodynamic radius depends not only on the particle size but also on the segment density. For open structures the ratio R_g/R_h is larger than unity. It decreases when the structure becomes more dense and should reach a limit for impenetrable hard spheres with $\rho = 0.778$. Experimentally, however, much smaller values were found for microgels. The particles appeared to be well swollen in a solvent, but the segment density in the periphery still was high such that the solvent molecules stayed captured. In other words, even this periphery remained largely nondrained. In microgels this effect can be pronounced such that the hydrodynamically effective radius can take values 3 times larger than the geometrically defined radius of gyration.[18] Exactly this behavior was found for the TMSC aggregates, giving evidence for a structure similar to microgels. The ρ parameter also depends on polydispersity and increases with the width of the size distribution. The size distribution was determined for some samples by the Laplace inversion with the CONTIN program.[15] One example of time correlation functions at various scattering angles is shown in Figure 6. The corresponding distributions of the hydrodynamic radius are given in Figure 7. The weak dependence of the apparent hydrodynamic radius is probably caused by the large polydispersity but may also result from internal segment motions that are superimposed to the translational diffusive motion. The size distribution is remarkably broad. Therefore, the observed small ρ values cannot be caused by the polydispersity.

Apparent Density of the Particles. It is instructive to have a closer look at the absolute values of the apparent density which is given by the equation

$$d_{app}(\mathrm{DS}) \equiv \frac{M_w(\mathrm{DS})/N_A}{4\pi/3R_g^3(\mathrm{DS})} \tag{8}$$

and is plotted in Figure 8. The apparent density increases dramatically with the DS, but even for DS 3.0 the apparent density $d_{app}(3.0) = 0.01$ g/mL is about 50 times smaller than the expected real density of the material. Hence, even this structure is highly swollen, probably only in the outer shell of dangling chains.

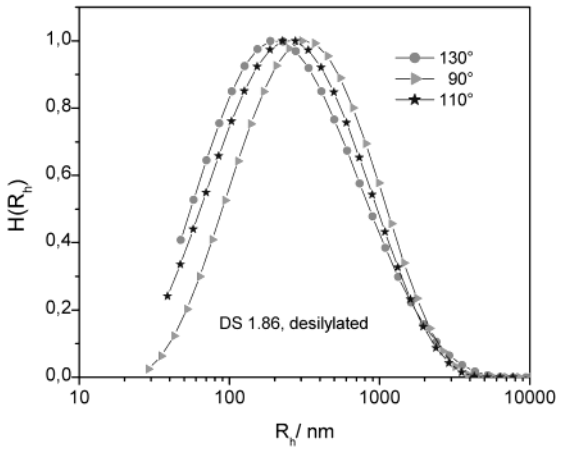

Figure 7. Hydrodynamic radii distributions of the same sample as in Figure 6. The slight shift of the maximum toward smaller values when the scattering angle is increased results from segmental motions.

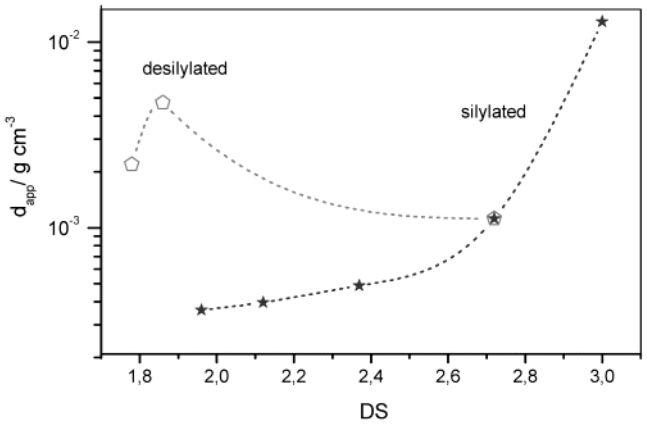

Figure 8. Apparent density for the samples from AVICEL-101 of different degrees of substitution.

Again, TMSC samples from desilylation showed different behavior. The apparent density strongly increased with increasing DS and was by a factor of 5−10 higher than that of a sample from silylation with similar DS.

Internal Structure. Scattering methods have the advantage of providing information not only on the shape of the particles but also on the internal structure. Every pair of scattering elements, i.e., monomer units, contributes to the scattering intensity; large distances or globular properties give their main contribution at small q values, but the contributions from short distances are recognizable at large q values. This asymptotic part is sensitive to differences in structure. A rod displays an asymptote very different from that of a hard sphere. There are two procedures to emphasize this asymptotic part of the angular dependent scattering curve: (i) the Kratky plot[19] in which the particle scattering factor $P(u)$ is multiplied by $u^2 = (qR_g)^2$ and (ii) the Casassa−Holtzer plot[20−22] where $P(u)M_w$ is multiplied by q/π. In both cases the q values or the scaled, dimensionless u value, can be used as independent parameter. The first plot is useful when compact structures are present; the second is suitable if the particle contains rigid structural elements. Both plots proved to be informative for the structures of aggregated TMSC particles.

Kratky Plot and Kuhn Segment Length. Figure 9 shows the scattering curves in the form of normalized Kratky plots. For comparison, the theoretical line of the

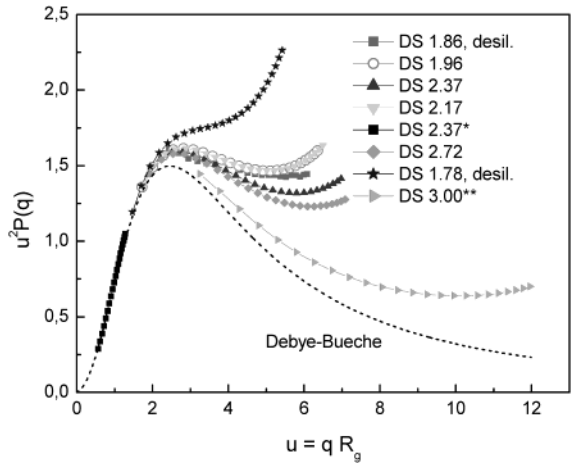

Figure 9. Kratky plots of the particle scattering factors at zero concentration of the various samples. The position at which a marked increase starts again may be related to the length of a Kuhn segment.

Debye−Bueche[23] model is added. This model corresponds to very large hyperbranched materials with many short dangling chains in the outermost shells.[24] Randomly branched or randomly aggregated chains approach an asymptotic plateau at $u^2P(u) \rightarrow 3.0$ for poor solvents that increases further with a power of 0.2 in a thermodynamically good solvent.[25] All TMSC curves show similar behavior with a tendency of a shift toward the Debye−Bueche model, which correlates with the DS of the silylated samples. But the desilylated samples do not fit this frame. The similarity to the Debye−Bueche curve clearly indicates an aggregated structure that excludes random aggregation.

The second striking feature of the curves is the upturn at large u values. This upturn is most pronounced for TMSC 1 (DS 1.78) and resembles semirigid chains. By linear extrapolation of the scattering function from medium toward large u values, and from large u to smaller ones, respectively, an intersection point is obtained. For linear chains this intersection point u^* is related to the Kuhn segment length l_K of a semirigid linear chain which is given as

$$q^* = \frac{u^*}{R_g} = \frac{12}{\pi l_K} \tag{9}$$

If we assume validity of this relationship also for the aggregated TMSC samples, we obtain the values of Table 2. The data form three groups. (1) Up to DS 2.72 the silylated samples have approximately the same values of $l_K = 122 \pm 2$ nm; (2) the Kuhn segment length of the two desilylated samples is with $l_K = 134 \pm 3$ nm about 10% longer, but (3) for the fully substituted sample of DS 3,0 the Kuhn segment is with $l_K = 174$ nm considerably larger. Evidently, a side-by-side alignment impeded segmental motion and thus led to an increasing rigidity.

Casassa−Holtzer Plot and Lateral Alignment. The structure of these rodlike Kuhn segments can be further analyzed in the nonnormalized Casassa−Holtzer plot.[20−22] For rigid rods a plateau is asymptotically approached from below to value of

$$(q/\pi)M_wP(u) \rightarrow M_L \tag{10}$$

where $M_L = (M_w/L_w)$ is the linear mass density and L_w

Table 2. Characteristic Structure Parameters Obtained from the Angular Dependence of the Scattered Light[a]

no.	DS	R_g/nm	u^*	q^*/ nm^{-1}	l_K / nm	$\langle l_K \rangle$/nm	M_L/(g/(mol nm))	n
1	1.78	157	4.6	0.029	131	134 (desilylated)	≈16000	(14)
2	1.86	176	5.0	0.028	136		15322	12.2
3	1.96	184	5.7	0.031	123	122 (silylated)	2366	1.83
4	2.12	188	5.7	0.032	119		2685	1.96
6	2.37	202	6.0	0.030	124		2995	2.09
7	2.72	2.5	6.3	0.031	123		6158	4.05
8	3.00	359	7.8	0.022	174	174	8574	5.40

[a] $u = qR_g$; the asterisk indicates the break in behavior in Figure 9, $q = (4\pi n_0/\lambda_0)\sin(\theta/2)$ with θ the scattering angle. q^* is related to the Kuhn segment length $l_K = 12/(\pi q^*)$; $M_L = (M/L)_w$ linear mass density with L the contour length of the rodlike particle, n = number of laterally aligned chain sections.

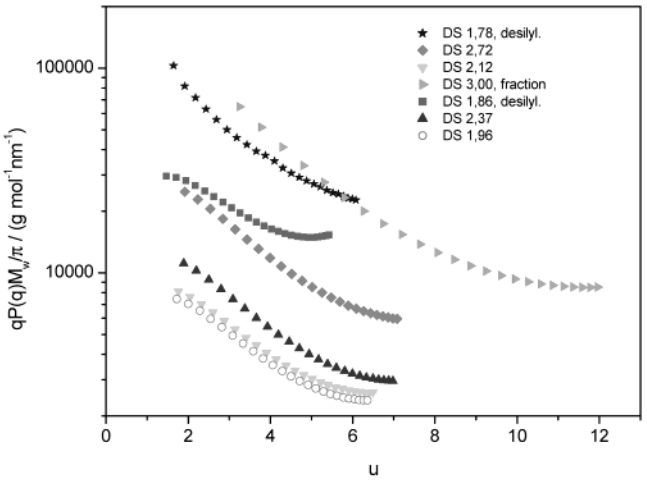

Figure 10. Nonnormalized Casassa−Holtzer plot of the scattering curves from the same TMSC samples as given in Figure 9. The plateau height at large u values gives the linear mass density M_L. The number of laterally aligned chains is obtained from the ratio of this to that of a single chain (see Table 2).

is the weight-average contour length. The corresponding value for individual chains can be calculated from the molar mass of the repeating unit and its length l_0 as $M_{L0} = M_0/l_0$ with $l_0 = 0.515$ nm. The data for the different DS are given in Table 2. According to Figure 10, the rod plateau is reached for almost all samples with the only exception of the desilylated sample of DS 1.78, where the radius of gyration was too small. But even here a plateau can roughly be estimated, which is given in brackets in Table 2. In all cases the measured linear mass density is significantly higher than that for a single chain. Evidently, the ratio $n = M_L/M_{L0}$ is a measure of side-by-side laterally aligned chain sections to form a bundle. Up to a DS of 2.4 lateral aggregation increased only weakly from 1.8 to 2.1 chains, on average. Then a jump to about 4.1 chains occurred for DS 2.72 and increased further to about 5.5 chains for DS 3.0. The highest number of laterally aggregated chains was observed for samples from desilylation where 12 to 14 laterally aligned chains were found.

Conclusions

The global properties already gave indication to aggregation which grew in size with the DS. Surprisingly, the aggregation became more pronounced when the samples were partially desilylated. Because of the large molar mass and radius of gyration of the various samples, a detailed analysis of the static and dynamic light scattering data was possible. This confirmed a densely packed structure but in addition revealed the presence of fairly rigid sections with Kuhn segment lengths of 122 nm up to 174 nm (for comparison: polystyrene has $l_K \approx 2$ nm, and the molecularly dissolved cellulose tricarbanilate has $l_K \approx 22$ nm). These segments are partially aligned side-by-side to form bundles containing 2−6 chains. These act as branching points as it is known from many other linear polysaccharides which can undergo thermally reversible gelation (see, e.g., Clark and Ross-Murphy[26]).

Taking into consideration the rather low apparent density, we can propose a model. The particles resemble branched macromolecules in which 2 to 6 from different chains rigid chain sections with a length of about 125 nm form bundles which act as junction zones. Bundle formation increases with the degree of substitution and is probably the main reason for the pronounced increase in the overall aggregation number with increasing DS.

Unexpectedly, desilylation causes a much stronger bundle formation and overall aggregation. This incites the following speculations. Lateral alignment becomes favored if the Kuhn segments are regularly substituted, probably with DS ≈ 3. These Kuhn segments are very likely the highly substituted segments in the cellulose chain because the lateral aggregation increased with the DS. On desilylation the chain sections that are not involved in lateral alignment are predominantly modified. This causes a chemical regularization in terms of nonpolar trimethylsilylated sequences. Possibly this discrimination of polar and nonpolar chain sections strongly favors bundle formation.

Chain sections that are not incorporated in the bundles are largely free in their segmental motions, but not in the bundles. Because of this mobility of dangling chains, the entropy of dilution is increased beyond the unfavorable enthalpy and dissolution occurs.[27] With increased lateral bundle formation the entropy of dilution is considerably diminished, and solubility becomes poorer. The particles will further aggregate until the aggregates contain enough dangling chains which via their entropy of mixing now overcome the attractive enthalpic interaction, and colloidal solubility is obtained.

Acknowledgment. We are indebted to the Deutsche Forschungsgemeinschaft (Schwerpunktprogramm Cellulose und Cellulosederivate−molekulares und supramolekulares Strukturdesign) for financial support.

References and Notes

(1) Schuyten, H. A.; Weaver, J. W.; Reid, J. D.; Jurgens, J. F. *J. Am. Chem. Soc.* **1948**, *70*, 1919.
(2) Mormann, W.; Demeter, J. *Macromolecules* **1999**, *32*, 1706.
(3) Mormann, W.; Demeter, J.; Wagner, T. *Macromol. Chem. Phys.* **1999**, *200*, 693.
(4) Mormann, W. *Cellulose*, in press.
(5) Petzold, K.; Koschella, A.; Kemm, D.; Heublein, B. *Cellulose*, in press.

(6) Mormann, W.; Wagner, T. *Macromol. Rapid Commun.* **1997**, *18*, 515.
(7) Mormann, W.; Demeter, J. *Macromol. Chem. Phys.* **2000**, *201*, 1963.
(8) Kamide, K.; Saito, M. *Eur. Polym. J.* **1984**, *20*, 903.
(9) Schulz, L.; Burchard, W.; Dönges, R. In Heinze, T. J., Glasser, W. G., Eds.; *Cellulose Derivatives, Modifications, Characterization and Nanostructures; ACS Symp. Ser.* **1998**, *688*, 218.
(10) Zimm, B. H. *J. Chem. Phys.* **1948**, *16*, 1099.
(11) Berry, G. C. *J. Chem. Phys.* **1966**, *44*, 4550.
(12) Berne, B. J.; Pecory, R. *Dynamic Light Scattering;* Wiley & Sons: New York, 1976.
(13) Einstein, A. (a) *Ann. Phys.* **1905**, *17*, 549. (b) Ph.D. Thesis, University of Zürich, 1905.
(14) Williams, G.; Watts, D. C. *Trans. Faraday Soc.* **1979**, *66*, 80.
(15) Provencher, S. W. *Comput. Phys. Commun.* **1982**, *27*, 229.
(16) Daoud, M.; Martin, J. E. In Avnir, D., Ed.; *The Fractal Approach to Heterogeneous Chemistry;* Wiley & Sons: Chichester, 1992; pp 107−130.
(17) Burchard, W.; Schmidt, M.; Stockmayer, W. H. *Macromolecules* **1980**, *13*, 1265.
(18) Burchard, W. *Chimia* **1985**, *39*, 10.
(19) Kratky, O.; Porod, G. *J. Colloid Sci.* **1949**, *4*, 35.
(20) Casassa, E. F. *J. Chem. Phys.* **1955**, *23*, 596.
(21) Holtzer, A. J. *J. Polym. Sci.* **1955**, *17*, 433.
(22) Denkinger, P.; Burchard, W. *J. Polym. Sci., Phys. Ed.* **1991**, *29*, 589.
(23) Debye, P.; Bueche, A. M. *J. Appl. Phys.* **1949**, *20*, 518.
(24) Burchard, W. *Adv. Polym. Sci.* **1999**, *153*, 113.
(25) Trappe, V.; Burchard, W. (a) Local dynamics in branched polymers. In Pike, E. R., Abbis, J. B., Eds.; *Light Scattering and Photon Correlation Spectroscopy*; Kluver Acad. Pubs: Dordrecht, 1997; pp 141−160. (b) *Macromolecules* **1997**, *30*, 2365.
(26) Clark, A. H.; Ross-Murphy, S. B. *Adv. Polym. Sci.* **1987**, *83*, 57.
(27) Ballauff, M. *Macromolecules* **1986**, *19*, 1366.

MA0300286